The use of Heterogeneous Chemistry for the Characterization of Functional Groups at the Gas – Particle Interface of Soot and TiO$_2$ Nanoparticles

A. Setyan[a], J.-J. Sauvain[a] and M.J. Rossi[b*]

[a] Institut Universitaire Romand de Santé au Travail (IST), Université de Lausanne et Université de Genève, rue du Bugnon 21, CH-1005 Lausanne

[b] Labor für Atmosphärenchemie (LAC), Paul Scherrer Institut (PSI), OFLA008, CH-5232 – Villigen PSI, Switzerland

ABSTRACT

Six gases (N((CH$_3$)$_3$), NH$_2$OH, CF$_3$COOH, HCl, NO$_2$, O$_3$) were selected to probe the surface of seven combustion aerosol (amorphous carbon, flame soot) and three types of TiO$_2$ nanoparticles using heterogeneous, that is gas-surface reactions. The gas uptake to saturation of the probes was measured under molecular flow conditions in a Knudsen flow reactor and expressed as a density of surface functional groups on a particular aerosol, namely acidic (carboxylic) and basic (conjugated oxides such as pyrones, N-heterocycles) sites, carbonyl (R$_1$-C(O)-R$_2$) and oxidizable (olefinic, -OH) groups. The limit of detection was generally well below 1% of a formal monolayer of adsorbed probe gas. With few exceptions most investigated aerosol samples interacted with all probe gases which points to the coexistence of different functional groups on the same aerosol surface such as acidic and basic groups. Generally, the carbonaceous particles displayed significant differences in surface group density: Printex 60 amorphous carbon had the lowest density of surface functional groups throughout, whereas Diesel soot recovered from a Diesel particulate filter had the largest. The presence of basic oxides on carbonaceous aerosol particles was inferred from the ratio of uptakes of CF$_3$COOH and HCl owing to the larger stability of the acetate compared to the chloride counterion in the resulting pyrylium salt. Both soots generated from a rich and a lean hexane diffusion flame had a large density of oxidizable groups similar to amorphous carbon FS 101. TiO$_2$ 15 had the lowest density of functional groups among the three studied TiO$_2$ nanoparticles for all probe gases despite the smallest size of its primary particles. The used technique enabled the measurement of the uptake probability of the probe gases on the various supported aerosol samples. The initial uptake probability, γ_0, of the probe gas onto the supported nanoparticles differed significantly among the various investigated aerosol samples but was roughly correlated with the density of surface groups, as expected.

*Address of corresponding author:
Michel J. Rossi
Labor für Atmosphärenchemie LAC
Paul Scherrer Institut (PSI)
OFLA008
CH-5232 Villigen PSI - Switzerland
e-mail : michel.rossi@psi.ch

Introduction

Aerosol particles occurring in the lower atmosphere directly and indirectly affect the radiative forcing of the climate, atmospheric processes and the hydrological cycle [1]. In the planetary boundary layer aerosols have a primary role in air pollution and control atmospheric composition, visibility and human health on a regional and local scale [2,3]. Atmospheric aerosols affect the radiation budget by scattering and absorbing solar and terrestrial radiation and indirectly by acting as cloud condensation nuclei that consist of particles larger than 50-100 nm in diameter. However, the radiative effects not only depend on the spatial distribution of aerosols, but also on their size, shape and chemical composition that control their optical constants. The interfacial chemical properties of atmospheric particulates control their ability to act as cloud condensation or ice nuclei and are therefore of relevance to the global climate [1].

Recent epidemiological and toxicological studies have shown that particulate matter has a significant harmful effect on public health, but also on animals and plants. Particulate matter PM_{10}, $PM_{2.5}$ and PM_1 which comprise particles whose effective aerodynamic diameter is smaller than 10.0, 2.5 and 1.0 µm, respectively, is sampled in the field on a routine basis. A small fraction of PM_1, predominantly the ultrafine fraction of less than 100 nm in diameter, is thought to spontaneously cross cellular membranes, both *in vitro* and *in vivo*, a process called translocation [4,5]. However, to date the molecular mechanism by which the fine (< 1 µm diameter) and ultrafine (< 0.1 µm) fraction cross cellular borders is not known with certainty. This translocation phenomenon has been related to mounting evidence that small particles cause adverse health effects such as cancer, respiratory and cardiovascular diseases, despite some reports to the contrary [6]. It is the submicron ultrafine fraction of particles that reportedly represents the highest health risk owing to their dimensions that are significantly smaller than the characteristic size of cells and bacteria [7]. As a consequence, a new field dealing with the toxicology of the ultrafine fraction of aerosols and nanoparticles has recently emerged that is called "nanotoxicology" [8].

Both the size of atmospheric aerosol particles as well as their surface chemical properties are important for their biological effects and adhesion. It still is an open question whether the particle surface area or the particle mass is the critical parameter that correlates with various health outcomes. There are results supporting either, surface or volume (mass), and a couple of particularly convincing examples in favor of surface scaling has been presented

by Oberdörster et al. [8]. Field studies frequently reveal that the number concentration of the submicron fraction of atmospheric particles is significantly higher than the supermicron fraction. The fact that the particle surface area decreases more slowly with the particle diameter than the volume (or mass) has led to the suggestion that it is the surface rather than the particle mass that is the critically important parameter for the harmful effects of submicron or nanoparticles. Beyond the choice "surface area or mass" the question of the particle surface composition and its effect on biological membranes and solid supports has hardly been raised in the literature. The characterization of the particle interface in terms of its physical and chemical properties is key to the understanding, and therefore control of the interaction between a nanoparticle and its substrate on a molecular level. The knowledge of nanoparticle chemical properties at the interface is also of importance in biological work where assays and *in vivo* experiments will be affected by it [9,10].

The present work deals with the application of a heterogeneous gas-surface titration technique in order to afford an alternative quantitative characterization of the interface of nanoparticles. It uses different probe gases that heterogeneously interact with the functional groups present at the nanoparticle interface and implies the measurement of the probe gas uptake until saturation. The results are expressed as a surface density of chemical functionalities such as acidic, basic, carbonyl and oxidizable groups if the particle metrology such as the particle size distribution function or some other metric for the total internal and external surface is known. This highly surface sensitive and specific chemical "interrogation" of the particle complements other techniques performed on environmental particulate matter such as X-Ray Photoelectron Spectroscopy (XPS), Time-of-flight Chemical Ionization Mass Spectrometry (TOFCIMS) and various high resolution imaging techniques [11,12]. Work on "chemical interrogation" of the complex interface of combustion aerosol and ultrafine particles such as TiO_2 has been performed some thirty years ago by Boehm and his group using liquid phase reagents that specifically reacted with interfacial functional groups in suspensions of particulate matter in tens of gram quantities [13] and has been critically reviewed in the recent past by Boehm [14,15].

This work deals with gas phase probe molecules that specifically interact with the interface of nanoparticles and has the clear advantage that it does not perturb the state of aggregation of the aerosol particles [14]. The central working hypothesis is the assumption that it is the unknown identity and abundance of functional groups at the interface of nanoparticles

that are responsible for their reactivity, both in the gas- as well as in the condensed phase including biological environments. We hereby propose a direct gas-phase titration technique with the following advantages: (a) it enables the use of MS-based techniques sensitive to less than one per cent of a molecular monolayer; (b) the low sample mass requirement in the range of one mg or so directly enables the investigation of ambient aerosol samples or from smog chambers; (c) the present approach emphasizes the measurement of interfacial or subsurface physical and chemical properties of nanoparticles not easily performed by spectroscopic methods, especially when molecular information is required. Setyan et al. [16] have recently successfully used this technique for the investigation of aerosols sampled in the field.

Experimental

Surface titration under molecular flow conditions using a Knudsen flow reactor.

The deposited powder samples have been "interrogated" by the probe gases at ambient temperature using a Knudsen flow reactor whose use for kinetics has been pioneered by Golden, Spokes and Benson [17]. Briefly, the method rests upon measuring the rate of disappearance of a gas under molecular flow conditions in the presence of a reactive substrate in comparison with its rate of effusion from the flow reactor that is measured under the relevant flow conditions. All experiments have been performed using a Knudsen flow reactor equipped with effusive molecular-beam phase sensitive mass spectrometric (MS) detection based on electron-impact ionization. The used two-chamber version adapted to the study of heterogeneous reactions has been described in detail in the recent literature [17,20]. The gas flow metered from a gas-handling vacuum line subsequently reacted with the sample once the isolation plunger was lifted. The kinetics are expressed as a heterogeneous rate constant k_{het} that depends on the surface-to-volume ratio A_s/V of the specific measurement system or as a dimensionless uptake coefficient γ that has been normalized by A_s/V, where A_s is the geometric surface area of the support and V the volume of the flow reactor. From the rate of disappearance of the probe gas, the heterogeneous rate constant k_{het} as well as the dimensionless corresponding uptake coefficient γ is given in the following equations:

$$k_{het} = (I_0/I - 1)k_{esc} \tag{1}$$

$$\gamma = k_{het}/\omega = (4/\bar{c}) \, k_{het} \, (A_s/V)^{-1} \tag{2}$$

where I_0 and I are the rectified amplitudes of the MS signals of the chopped molecular beam recorded by the lock-in amplifier in the absence and presence of the sample, respectively, and $\omega = (\bar{c}/4V)A_s$ is the calculated gas-surface collision frequency of the average molecule moving at a mean molecular speed $\bar{c}$. Equation (2) shows the normalization of k_{het} by A_s/V in order to obtain the dimensionless γ.

The specific parameters of the used Knudsen flow reactor are given in Table 1. The emphasis of the present work is on the time integral of the net loss of the probe gas to the reactive substrate and represents the total number N_i^M of probe gas molecules M lost on the particular sample by uptake:

$$N_i^M(\text{aerosol} + \text{support}) = \int(F_M^i - F_M(t))dt \tag{3}$$

where F_M^i and $F_M(t)$ are the measured molecular flow rates flowing into and escaping the flow reactor. The integration period from $t = 0$ to t is determined by the time interval it takes to saturate the sample completely, that is until no more uptake is experimentally measurable and $F_M^i = F_M(t)$. The raw data $N_i^M(\text{aerosol} + \text{support})$ are corrected for the uptake $N_i^M(\text{support})$ of the probe gas on the empty FEP-Teflon-lined sample dish according to equation (4) and yield $N_i^M(\text{aerosol})$, or in short N_i^M, in molecular units. It is presented as either normalized to mass (number of molecules/mg) or to the total internal and external surface area of the sample measured according to BET (number of molecules/cm^2 of aerosol surface):

$$N_i^M(\text{aerosol}) = N_i^M(\text{aerosol} + \text{support}) - N_i^M(\text{support}) \tag{4}$$

The BET surface has been taken as a metric of the total internal and external surface when normalizing $N_i^M(\text{aerosol})$ because the probe gas has sufficient time to interact with the total internal and external surface area of the sample up to complete saturation of the total surface area. The BET adsorption isotherm does not routinely lead to a distinction between the external and internal surface or between pores of different sizes, except when data on the hysteresis behaviour of adsorption are included. In contrast, the uptake kinetics is normalized to the geometric surface area owing to the fact that γ is usually measured right after the start of exposing the sample to the probe gas (γ_0). One may regard $N_i^M(\text{aerosol})$ as a lower limiting value if the BET surface would overestimate the "true" surface, whereas $\gamma(\gamma_0)$ may be regarded

as an upper limiting value if it is based on the geometric surface area of the sample or its projection onto the sample support.

Source of Materials.

Unless otherwise noted, all materials of commercial origin have been used as received. The following three samples of commercially available amorphous carbon from Evonik (Frankfurt am Main, Germany, formerly Degussa AG) have been used: FS 101, Printex 60 and FW 2 whose physical and chemical properties are listed in the brochure "Pigment Blacks" (Pigmentrusse/pigment blacks Technische Daten Europa/Technical Data Europe, Degussa AG, Advanced Fillers & Pigments, 2006). The soot standard reference material SRM 2975 has been obtained from NIST in gram quantities and has been collected from a Diesel engine of a heavy duty industrial forklift. It is accompanied by a certificate exhibiting all measured properties. Deposited Diesel soot from a heavy duty urban bus engine of a Swiss Transit Authority (TPG) has been recovered from a Diesel Particulate Filter (DPF-CRT) in a bus maintenance yard [16]. This sample has been called "Diesel TPG". Soot from a laboratory flame using a diffusion burner operating on n-hexane has been obtained at two operating conditions, namely "rich" and "lean" combustion conditions using a co-flow device whose design and operation have been published before [18,20]. For the generation of soot from a rich hexane flame a porous glass plug made of a Pyrex disc enabling liquid fuel transport from the reservoir to the flame across capillaries in the range 41-100 μm (Verrerie de Carouge, porosity 2) and an air flow rate of 1.375 l min^{-1} have been used. The lean flame was maintained using a porous glass plug of 11-16 μm wide capillaries (Verrerie de Carouge, porosité 4) and an air flow rate of 1.75 l min^{-1}. The flame soot was directly deposited onto a glass Petri dish of 4 cm ID and weighed gravimetrically, typically several mg. Although the combustion stoichiometry of the rich and lean hexane flame were very similar, we have used the products of the heterogeneous reaction of NO_2 on the corresponding soot as a discriminating feature [18,21]. The criterion between a rich and lean hexane flame was the exclusive HONO production resulting from the heterogeneous reaction on soot from the rich and NO generation from the lean flame [18,21]. In order to control the quality of soot on a routine basis frequent checks using the Knudsen flow reactor have been performed. References 18 and 20 provide further details on the soot properties.

Two TiO_2 samples were purchased from Sigma-Aldrich: TiO_2 anatase (art. no. 637254, hereafter called "$TiO_2$15") and TiO_2 mixture of rutile and anatase (art. no. 634662,

hereafter called "TiO$_2$ 50"). TiO$_2$ 15 and TiO$_2$ 50 had primary average particle diameters of 15 and 25-75 nm. TiO$_2$ P25, an often used catalyst support of technical significance, was purchased from Evonik (Degussa) and consisted of 21 nm wide particles on average. TiO$_2$ 15, TiO$_2$ 50 and TiO$_2$ P25 contained 98, 65 and 80-90% (w/w) anatase balanced by rutile. The mass of the powder samples were measured gravimetrically and subsequently spread out on the FEP-Teflon (Dupont Inc., Geneva)-lined Pyrex sample dish. The uptakes to saturation by the probe gases were independent of the way the samples were spread out on the sample support.

Surface Probe Molecules and Uptake Experiments.

The six probe molecules used are trimethylamine (N(CH$_3$)$_3$), hydroxylamine (NH$_2$OH), hydrochloric acid (HCl), trifluoroacetic acid (CF$_3$COOH), nitrogen dioxide (NO$_2$) and ozone (O$_3$). N(CH$_3$)$_3$ and CF$_3$COOH were purchased from Sigma-Aldrich (purum $\geq$ 99% and puriss., respectively), NO$_2$ and HCl were obtained from Carbagas. NH$_2$OH is prepared by thermal decomposition of hydroxylammonium phosphate ((NH$_3$OH)$_3$PO$_4$) according to the method of Schenk [22]. Small aliquots of the solid salt were decomposed inside a vacuum inlet line prior to use in order to avoid the reaction of free NH$_2$OH with air. Ozone was generated in a Fischer ozone generator from pure O$_2$. The resulting O$_2$ flow containing 5-10% O$_3$ in O$_2$ was passed across a silicagel trap held at 196 K in order to freeze out O$_3$ whose vapor pressure was controlled using a cold methanol slush bath at 193 K when filling a storage bulb. All samples except O$_3$ have been distilled trap-to-trap using a greaseless vacuum inlet line as a routine purification procedure.

Figures 1 and 2 provide typical examples of uptakes of acidic probe gases on amorphous carbon FW 2 and TiO$_2$ P25, respectively. The sharp drop in MS signal at m/e 45 (COOH$^+$) and 36 (HCl$^+$) is a consequence of exposing the sample compartment to the probe gas that obviously has a strong interaction with the respective substrate. Figures 1 and 2 clearly show that the gas uptake saturates after several hundred seconds, depending on the flow rate or partial pressure in the flow reactor. The small decrease of the I$_0$ level of the probe gas MS signal before opening and after closing the sample compartment is due to the decrease of the stagnant pressure in the vacuum line of the gas inlet. Figures 3 and 4 show typical examples of uptakes of N(CH$_3$)$_3$ and O$_3$ on amorphous carbon FS 101 and on soot from a rich hexane flame monitored at m/e 58 (C$_3$NH$_8^+$) and 48 (O$_3^+$), respectively. A look at Figure 4 shows that the O$_3$ uptake is not quite saturated after t = 1090 s, a behaviour we have observed previously for ozone interacting with Norit A charcoal [23]. We therefore have to regard the O$_3$

uptake on hexane flame soot as a lower limiting value which should be to within 15% or so of the fully saturated value akin to the O_3/charcoal case.

The probe molecules taken up are converted into N_i^M(aerosol) values according to equations (3) and (4) and are listed in Table 2 which displays the results for all investigated carbonaceous and TiO_2 aerosols. Results obtained for blanks (empty Petri dishes) indicate that the correction for the uptake of the probe gas on the blanks may be significant in some cases. Indeed, depending on the probe gas, between 1 and 50 % of the uptake occurs onto the blank. Among the worst case is the reaction of HCl with hexane soot (lean flame) where 65 % of the uptake is attributed to the blank. As toxicological studies frequently use mass as the particulate exposure metric, we have normalized the N_i^M(aerosol) values to mass (first row of each box in Table 2). As the surface density of functional groups may be more relevant than mass, we present N_i^M(aerosol) values normalized to surface area (BET, second row, Table 2). The values for the BET surface area of the used samples are either known from the manufacturer or have been measured using a Sorptomatic 1990 (Fisons Instruments) (N_2) typically using 50 - 100 mg of sample mass (see Table 2). A third way of expressing the results is in terms of a formal molecular monolayer (third row, Table 2). The estimated quantity of probe gas forming a monolayer (ML) was calculated from the bulk densities taken from the CRC Handbook [24] using the expression $ML = (\rho N_L/M)^{2/3}$, where ρ, N_L and M are the bulk density, Avogadro's number and molar mass, respectively. The following values for ML have been obtained: $1ML(N(CH_3)_3) = 3.6 \times 10^{14}$ molecule cm^{-2}, $1ML(NH_2OH) = 7.9 \times 10^{14}$ molecule cm^{-2}, $1ML(HCl) = 8.6 \times 10^{14}$ molecule cm^{-2}, $1ML(CF_3COOH) = 4.0 \times 10^{14}$ molecule cm^{-2}, $1ML(NO_2) = 7.1 \times 10^{14}$ molecule cm^{-2}, $1ML(O_3) = 7.4 \times 10^{14}$ molecule cm^{-2}. A look at Table 2 reveals that the data span a wide range of N_i^M(aerosol) values, from 0.81 ($N(CH_3)_3$/FS 101) to 364 % of a molecular monolayer (O_3/lean flame hexane soot).

The measurement of the heterogeneous rate constant for uptake of the probe gas, k_{het}, and the associated dimensionless uptake coefficient γ according to equations (1) and (2) are displayed in Table 3. The results were obtained under the assumption of a first order rate law for the uptake process based on the geometric surface area of the sample support (equation (2)). Owing to the very small masses of the solid substrate used, usually on the order of 1 to 3 mg, we may have to contend with the possibility that the sample will not form a coherent layer across the sample support such that we state an uncertainty of a factor of two in γ.

Results and Discussion.

Following our previous approach on the titration of interfacial functional groups on laboratory-generated aerosol particles by specific gas phase probe molecules [16,25] we emphasize that the present approach affords a broad classification of functional groups at the interface. These interact with the gas phase on the time scale of the experiment given by $1/k_{esc}$ (Table 1) on the order of 40 s or so. The six probe gases, $N(CH_3)_3$, NH_2OH, HCl, CF_3COOH, NO_2 and O_3 have been selected in order to obtain an idea on the identity of the interfacial functional groups of the supported nanoparticles. Here we deal with fairly well-defined aerosol particles rather than aerosols collected in the field [16]. These particles nevertheless display complexities depending on the way they were generated, usually through incomplete combustion in the case of amorphous carbon and soot, and through thermal oxidation in the case of TiO_2. For example, the organic phase of all carbonaceous samples listed in Table 2 may reveal hundreds of distinct organic compounds if subjected to detailed analytical separation and identification [26,27]. The gas-phase titration technique used here preserves the average particle morphology as well as the location of the functional group relative to the interface, thus emphasizing surface composition rather than the investigation of the bulk composition of the particle. Minimal perturbation of collected aerosols immobilized on filters or solid supports is desired, even mandatory, for many investigations. The intent and purpose of the present work is the identification of functional groups on the surface of carbonaceous or other nanoparticles such as –COOH (carboxylic), -C(O)- (carbonyl or aldehydic), oxidizable groups such as –OH being part of hydroquinone-like structures, olefinic moieties as well as acidic and basic oxides that do not necessarily contain nitrogen. For TiO_2 nanoparticles the surface functionalities consist of surface hydroxyl groups whose acidity ranges from very basic to very acidic, as well as reactive surface and subsurface defects and/or O-atom vacancies.

We stress that the present approach does not represent a proxy for the reactivity, in terms of both the rate and the reaction products, of aerosol particles in the condensed phase. Rather, the information gathered from the present approach will form the basis for an understanding of the reactivity of the aerosol interface in terms of the surface composition corresponding to surface functional groups reaching into the solution environment. Based on heterogeneous chemistry, the results enable a partial understanding of the reactivity of the aerosol at the aerosol-atmosphere interface. Moreover, we surmise that the aerosol interface composition will not significantly change when the aerosol particle is immersed into a liquid,

except perhaps for hydrolysis reactions, such that the results of the present approach may still give useful clues for solution studies.

One must ask the question whether the proposed reactions uniquely identify the surface functional groups in cases no reaction products are detected. Setyan et al. [16] come to the conclusion that the listed reactions are unique after consideration of other possible reactions of the gas phase probes. Three stringent conditions for the occurrence of a titration reaction under the present reaction conditions have to be met: The titration reaction must occur (a) rapidly on the time scale given by $1/k_{esc}$ (see Table 1); (b) at ambient temperature; (c) at low partial pressure or concentration, typically in the range $10^{11} - 10^{13}$ molecule cm^{-3}. Under these restrictive conditions only the reactions discussed below are thought to occur in the Knudsen flow reactor under the present conditions. A fourth requirement is that the probe reaction be irreversible on the time scale of the time required to saturate the interface. For each nanoparticle/trace gas combination a test was performed by halting the trace gas flow, evacuating the sample chamber and repeating the uptake at the same gas flow. In no case significant additional uptake has been observed in the second uptake experiment so that we conclude that indeed, uptake is irreversible on the stated time scale.

Carbonaceous Particles.

Trimethylamine is a strong base in the gas phase as measured by its proton affinity (PA = 942 kJ Mol^{-1} compared to 854 kJ Mol^{-1} for NH$_3$) [28] and is designed to probe strong as well as weak Lewis acidic interfacial sites according to reaction (5) in which the acidic site is represented by a carboxylic group:

$$-COOH + N(CH_3)_3 \rightarrow -COO^-(CH_3)_3NH^+ \tag{5}$$

This reaction is monitored by recording the loss of N(CH$_3$)$_3$ from the gas phase without detection of a reaction product owing to the formation of a salt. In addition to carboxylic groups there are other acidic groups that may contribute to the acidity of organic compounds such as acidic oxides on combustion aerosol particles that have been extensively studied in the past by Hofmann and coworkers [29] and Boehm and coworkers [30-32]. These will be discussed below in more detail.

The $N_i^{N(CH3)3}$(aerosol) values for trimethylamine displayed in Table 2 reveal a significant presence of Lewis acidic functional groups among all investigated carbonaceous nanoparticles. We strongly suspect the presence of carboxylic groups generated in the combustion process similar to the occurrence of mono- and dicarboxylic acids resulting from photooxidation processes of biogenic hydrocarbons that end up as secondary organic aerosols (SOA) [26,27,33,34]. There is extensive evidence from field studies for the presence of organic mono- and dicarboxylic acids, especially in aged (= oxidized) secondary aerosols (SOA) [35,36]. Although almost all investigations have so far only addressed the bulk phase of the sampled aerosols we make the assumption that carboxylic acids may also be found at the interface and are involved in the gas phase neutralization reaction with $N(CH_3)_3$. In addition, combustion aerosols may contain acidic oxides (see Scheme I), a subgroup of interfacial oxides on carbon, that have been detected on suitably activated amorphous carbon through heat treatment in the presence of dry oxygen [14,29,31]. Some of these acidic oxides may be the precursors of surface carboxylic groups in the presence of water vapour. In fact, Boehm and coworkers detect four different acidic surface groups, classified from I to IV [31]. Group I and II are identified as being a more and a less (lactone) acidic carboxylic group, respectively, with group III and IV being a phenolic and carbonyl group, respectively. Scheme I, image A and B present a molecular model for groups I and II before and after reaction with a base, whereas images C (lactol) and D display the complete molecular model with all four groups. These models are consistent with all chemical reactions occurring in solution which enable the identification of the surface functional groups present on activated charcoal or amorphous carbon. By analogy we conclude that the interfacial reaction of gas phase $N(CH_3)_3$ proceeds similarly to reaction of these acidic oxides with strong base in solution in view of the large gas phase proton affinity of $N(CH_3)_3$.

A closer look at the results for $N(CH_3)_3$ in Table 2 reveals low values of $N_i^{N(CH3)3}$(aerosol) of less than one per cent or so of a formal monolayer for the amorphous carbon samples as well as for hexane flame soot, both rich and lean flame. In contrast, $N_i^{N(CH3)3}{}_i$ values are high for FW2, on the order of a factor of ten larger than the foregoing akin to the "aged" Diesel soot samples SRM 2975 and Diesel TPG. According to the manufacturer's specifications the amorphous carbon FW 2 has been postoxidized using either HNO_3 or H_2O_2 which would explain the increased $N_i^{N(CH3)3}$ values compared to the other two samples, namely FS 101 and Printex 60. We take note that the "aged" Diesel soot samples SRM 2975 and Diesel TPG, both of which have been previously discussed [16,37] and which are

displayed in Table 2 for the sake of comparison, have an increased amount of acidic surface functional groups. A stability test of the trimethylammonium salt at the saturated interface of amorphous carbon FW2 after laboratory storage for three months inside a sealable polytheylene bag revealed a 20% decay using a repeated uptake experiment at a similar partial pressure of $N(CH_3)_3$. Based on these different studies, the general apparent sequence for the $N(CH_3)_3$ reactivity on different carbonaceous aerosol is the following:

"aged" Diesel soot (SRM 2975 and Diesel TPG); amorphous carbon FW 2 > amorphous carbon Printex 60; FS 101; lean and rich hexane soot

The reaction of hydroxylamine indicates the presence of carbonyl groups of aldehydes and ketones forming an oxime if catalytic amounts of organic acids are present as the reaction is general acid- or base-catalyzed [38]. The presence of catalytic amounts of acid seems to be necessary as a pure thin film of benzophenone failed to react under our experimental conditions [25]. The reaction occurs according to equation (6):

$$R^1R^2\text{-}C\text{=}O + NH_2OH \rightarrow R^1R^2\text{-}C(OH)(NHOH) \rightarrow R^1R^2\text{-}C\text{=}N\text{-}OH + H_2O \qquad (6)$$

Owing to the heterogeneous nature of the reaction under the present conditions the reaction may possibly also occur with carbonyl groups other than those of aldehydes and ketones: amides, organic acids, acid anhydrides and other carbonyl-bearing species could in principle also contribute to the reactivity towards NH_2OH. However, below we will present quantitative results that suggest that the presence of species other than aldehydes and ketones are unlikely which is in agreement with the results of Boehm [14].

The N_i^{NH2OH} values for the carbonaceous substrates displayed in Table 2 are significant and are at variance with the results of Demirdjian for toluene soot from a diffusion flame [25]. Of note is that the used co-flow burners for both toluene and hexane soot are of very similar design and operated under near identical flow conditions so that we expected soot of comparable properties [18,20]. The amorphous carbon samples all show low reactivity towards oxime formation upon NH_2OH exposure, whereas the aged Diesel particulate samples SRM 2975 and Diesel TPG show a large amount of oxime formation. Both hexane flame soot samples lie in-between the Diesel soot models and the amorphous carbons inasmuch as reaction with NH_2OH is concerned which is noteworthy in view of our previous results on

toluene flame soot which resulted in low values [25]. Printex 60 again shows the lowest reactivity and qualifies for a carbon substrate with a low number of surface functional groups. Owing to the fact that oxime formation is general acid catalyzed [38] the differential reactivity of the present carbonaceous samples may either be attributed to the availability or mobility of the acid or, more likely, to the number of available carbonyl groups at the interface. The elucidation of this aspect of surface titration must await further experiments as is the question regarding the types of surface carbonyl groups that are able to undergo oxime formation in addition to aldehydes and ketones. At this moment we rule out significant surface oxime formation by carboxylic groups because of the low $N_i^{N(CH3)3}$ values displayed in Table 2. These data suggest a surface density of carboxylic groups of less than a factor of ten compared to carbonyl groups.

An additional potential ambiguity concerns the basic nature of both NH_2OH and $N(CH_3)_3$, the former being a very much weaker base compared to the latter in both the gas phase (PA) as well as in solution (pK_a). If the N_i^{NH2OH}(aerosol) value were due to the basicity alone one would expect at most an identical, if not a smaller value compared to $N_i^{N(CH3)3}$(aerosol). In fact, just the opposite is true by factors of several up to ten which points to a very limited role of NH_2OH as a (weak) base when it interacts with the existing surface groups. An obvious exception is that of FW2 which has a large number of oxidized surface sites owing to its scheduled postoxidation treatment. We therefore tend to attribute the high reactivity of the aerosol surface towards NH_2OH to oxime formation according to equation (6), aldehydes and ketones being the sole carriers of oxime formation. Owing to the fact that carbonyl groups represent a functional group whose formal oxidation number is lower than for a carboxylic group we may state that NH_2OH primarily interacts with aerosol particles whose surface is partially oxidized. In contrast, the reaction with $N(CH_3)_3$ signals the presence of a totally oxidized interface mostly consisting of carboxylic groups.

Acidic probe gases such as HCl and CF_3COOH interact with interfacial Lewis base sites B: whose molecular identity is not known *a priori*. Equation (7) displays the expected acid-base reaction with the generation of the acid-base complex or salt:

$$B: + HCl/CF_3COOH \rightarrow B:H^+Cl^-/CF_3COO^- \qquad (7)$$

In discussing acidities or basicities of surface functional groups we find it more appropriate to consider the corresponding gas phase rather than the solution values because the interface lacks extensive solvation capabilities, at least under the present experimental conditions of high vacuum and the extremely low relative humidites. A rigorous proof for this assumption cannot be given at this time except to state that this concept enables several explanations of observations that are not possible when solution properties are used. It is noteworthy that HCl is a weaker acid than CF_3COOH in the gas phase in contrast to aqueous solution where solvating effects predominate [28]. Owing to the smaller proton affinity compared to Cl^-, CF_3COO^- is less basic than Cl^- (1350 vs. 1395 kJ Mol^{-1}). Therefore, the gas phase acidity of the conjugate acid HCl is lower than that of CF_3COOH. The basic sites may be embodied by basic oxides whose existence on combustion aerosol particles and associated reactivity have been extensively documented in the past [29,39-42]. The basicity does not need to be centered on a N-containing base such as an amine or pyridine, rather it may be located on O-containing "bases" or basic oxides such as displayed in Scheme II. Indeed, relevant acid-base reactions of α - and γ - pyrones that serve as model compounds for the basic oxides with HCl and CF_3COOH lead to pyrylium salts upon neutralization (Scheme II). In addition to the fact that certain carbonaceous substrates do not interact with either CF_3COOH or HCl (see Table 2), the reactivities of the acidic probe gases with the basic oxides are in general lower than for the corresponding basic $N(CH_3)_3$ probe. According to Table 2 SRM 2975 and Diesel TPG soot do not react with CF_3COOH whereas all three amorphous carbons FS 101, Printex 60 and FW 2 do. For the HCl probe, the inverse is true: FS 101 and FW 2 do not interact, Printex 60 does so marginally, whereas both SRM 2975 and Diesel TPG abundantly react with HCl.

Basic oxides are generated when amorphous carbon is heated under dry conditions to 900°C and subsequently exposed to a humid atmosphere at ambient temperature [13,39]. Depending on specific combustion conditions such as temperature, richness of flame and residence time it is not inconceivable that certain amorphous carbons may accumulate basic oxides on their surface. Boehm and coworkers have found that acetic acid (CH_3COOH) is taken up on basic oxides located on the surface of amorphous carbon in quantities larger by a factor of three to six compared to HCl [39]. We attribute this to charge delocalization in the acetate compared to the chloride ion thus rendering it more nucleophilic than acetate. The rate of the reverse reaction in equation (7) will therefore be faster for Cl^- than for CH_3COO^-, thereby shifting the equilibrium towards the acid-base complex (salt) for acetate compared to

chloride. This may be explained by the fact that the reaction kinetics of $CH_3COO^- + H^+ \rightarrow CH_3COOH$ is slower than $Cl^- + H^+ \rightarrow HCl$ owing to charge delocalization in the acetate anion. This in turn will affect the equilibrium in equation (7) in agreement with the results of Boehm and coworkers [39]. We therefore take the ratio $N_i^{CF3COOH}/N_i^{HCl} > 1$ as an indication for the presence of basic oxides on the surface of these carbonaceous aerosol particles which does not preclude the presence of additional types of Lewis bases on the substrate at the same time. CF_3COOH which has been used as a probe gas is a much stronger acid in solution compared to CH_3COOH which has been used by Böhm and Voll [39]. Nevertheless, we expect a similar degree of delocalization, hence similar stabilization of the negative charge in both trifluoroacetate and acetate anion in view of their similar structure.

Considering the above ratio from data displayed in Table 2 we conclude that all the investigated amorphous carbons, namely FS 101, Printex 60 and FW 2 and to a lesser extent hexane soot from a lean flame apparently contain basic oxides on their surface by virtue of the larger uptake of CF_3COOH compared to HCl. Interestingly, Setyan and coworkers [16] have investigated a secondary organic aerosol generated from photooxidation of limonene, a naturally occurring terpene ($C_{10}H_{16}$). In this case the ratio $N_i^{CF3COOH}/N_i^{HCl}$ amounts to a factor of ten and indicates the presence of basic oxides despite the fact that the aerosol was generated from photooxidation, whereas all aerosol substrates studied here have been generated from thermal oxidation or combustion. In contrast, both "aged" Diesel soot substrates as well as soot from the rich hexane flame take up higher amounts of HCl than CF_3COOH. The same observation has been made for PM_4 collected in the field [16]. Diesel TPG soot is noteworthy for its high absolute value of N_i^{HCl}(aerosol) in that it can bind significant amounts of HCl compared to all other substrates. Moreover, the same substrate also contains a large number of acidic sites (see Table 2) in just about equal numbers. This shows that a soot surface may contain a large number of Lewis base as well as acidic surface functional groups that act independently of each other. A last remark concerns Printex 60 soot that once again shows a low number of basic sites compared to all other carbonaceous samples. In the end, the present titration technique does not give detailed molecular information on the sites reacting with both CF_3COOH and HCl. However, the ratio $N_i^{CF3COOH}/N_i^{HCl}$ reveals precious information on the possible presence of pyrone structures. Moreover, the structure and identity of the remaining basic sites preferentially reacting with HCl remain to be elucidated in the future.

Both O_3 and NO_2 are oxidizers that may specifically interact with oxidizable, thus reduced sites on combustion particles according to equation (8):

$$-C_{red} + O_3/NO_2 \rightarrow -C_{ox} + O_2/N(II\ or\ III)\ (HONO\ or\ NO) \qquad (8)$$

O_3 is a stronger oxidizer than NO_2, therefore the extent of interaction of an oxidizable substrate with ozone will usually be larger than with NO_2 (see Table 2). The reaction product of O_3 on carbonaceous aerosol particles is O_2 [23] and of NO_2 either HONO and/or NO [21], depending on the nature of the adsorbed organic phase. Olefins are practically the only hydrocarbons that quickly react with O_3 in gas phase ozonolysis reactions whose products and mechanism are well established [43]. In contrast, reactions of gas-phase polycyclic aromatic hydrocarbons (PAHs) with O_3 are slow, except in cases where part of the hydrocarbon retains an olefinic character, such as for example in azulene, acenaphthylene and indene [44-47]. In contrast, the reaction rate constant for the reaction of O_3 with PAH's adsorbed on SiO_2, graphite or Diesel soot is larger by two-to-three orders of magnitude compared to the corresponding reaction of gas phase PAH's [48-51] when the disappearance of the PAH in the presence of O_3 is monitored. The fundamental reason for this discrepancy is unclear at the moment, but it may be related to the nature of the adsorption site on the carbonaceous substrate. A significant fraction, namely up to 70% of the PAH's adsorbed on graphite and amorphous carbon resists oxidative decay in the presence of O_3, whereas the decay is quantitative for PAH's adsorbed on SiO_2 [48]. A similar situation holds for reactions of NO_2 with PAH's adsorbed on Diesel soot and silica whose competitive kinetics with OH free radical has been studied by Villenave and coworkers [52,53]. Slower by four orders of magnitude compared to OH, the NO_2/PAH reaction retains some structure-specific aspects but is deemed not to be of any atmospheric importance.

Concerning the interaction with O_3 and NO_2 both types of hexane flame soot generated in the laboratory from a diffusion flame have a functional group density larger by at least a factor of ten compared to all other carbonaceous substrates except FS101. In going from a rich to a lean hexane flame the result for NO_2 displayed in Table 2 is as expected, that is N_i^{NO2}(aerosol) for the rich flame soot is larger by a factor of two compared to the lean flame soot. We know that a rich hexane or decane flame generates an adsorbed organic phase that is less oxidized, hence interacts to a larger extent with NO_2 [18]. In contrast, when considering the analogous results for O_3 as a probe gas interacting with hexane flame soot the ordering is inversed with values differing by only 50%. Therefore, the reactivity of both hexane flame

soots towards O_3 is apparently very similar. Both the SRM 2975 as well as all three amorphous carbon samples have low N_i^{NO2} values indicating their advanced state of surface oxidation in contrast to hexane flame soot that may be characterized by a fairly reduced surface. An obvious exception is the Diesel TPG sample that apparently retains its reducing power despite its age, sample history and number of carboxylic groups based on $N(CH_3)_3$ uptake (see Table 2). In keeping with the relative oxidizing power of O_3 vs. NO_2, the N_i^{O3} values are larger by a factor of ten or more compared to NO_2 for the corresponding substrates.

Other methods of surface characterization of carbonaceous particles have been proposed such as surface-sensitive spectroscopic techniques [14,15]. However, these yield different answers compared to the presently used chemical interrogation of the particulate interface. A nice illustration of the capabilities of modern spectroscopic techniques at resolving microstructural details of the complex surface of carbonaceous particles has been presented by Schlögl and coworkers [54]. The combination of high-resolution imaging, electron energy loss spectroscopy and C1s and O1s XPS led to significant correlations between the degree of sp^2 and sp^3 hybridization of carbon, the size of the graphene layers, their curvature and the O-content of the interface. These microstructural details are a fingerprint of the soot samples that differ according to the source and the way they were generated by combustion and represent useful complementary structural information to the surface-chemical investigation performed in this work. An interesting attempt at identifying and quantifying the surface functional groups of amorphous carbon (soot) was undertaken by Muckenhuber and Grothe [55,56]. These workers used both temperature-programmed desorption MS (TPDMS) as well as Diffuse Reflectance FTIR Spectroscopy (DRIFTS) as diagnostic techniques after heterogeneous reaction of soot with the mild oxidizer NO_2 at temperatures up to 400°C. The thermal stability of the various generated surface functional groups after mild NO_2 oxidation was subsequently probed by TPDMS and DRIFTS for the identification of the gas phase oxidation products and the remaining surface intermediates, respectively. The reaction with NO_2 occurs at the interface and leads to the formation of an acidic functional group that decomposes into CO_2 and NO at 140°C. DRIFTS successfully identified the precursor to this acidic group but not the group itself because of its rapid thermal decomposition. In parallel, quantum mechanical calculations are beginning to address the thermal decomposition of oxidized graphenic soot platelets as reaction products from functionalized polycyclic aromatic hydrocarbon oxidation in order to support the interpretation of TPDMS experiments [57].

TiO$_2$ aerosol particles.

In contrast to nanoparticle properties much knowledge has accumulated on the structure, physics and surface/bulk chemistry of single crystal TiO$_2$ which has recently been summarized by Diebold [58]. We therefore take the single crystal properties of TiO$_2$ as a limiting behaviour for nanoparticles in terms of reactive surface sites that consist of oxygen vacancies as well as surface defects. These oxygen vacancies on the surface of single crystal TiO$_2$ corresponding to penta-coordinated Ti^{3+} ions are bridged with reactive surface hydroxyl groups after exposure to water vapor that dissociatively chemisorbs [58]. These oxygen vacancies constitute approximately 5 to 10% of the surface area on the (110) face of rutile which we consider a lower limiting value for TiO$_2$ nanoparticles. In addition, subsurface O-vacancies and structural defects are important as they migrate towards the surface and participate in the reactivity of the TiO$_2$ single crystal surface depending on several experimental parameters such as temperature and diffusion coefficients of these defects. It seems therefore, that surface and bulk properties in TiO$_2$ may not be viewed separately and that, apart from structural defects, the only chemically distinguishable surface functional group is (bridging) surface hydroxyl whose acidic properties span a wide range [58]. Titania (TiO$_2$) has therefore both surface –OH groups as well as Lewis acid corresponding to structural defects, but no Brönsted acid sites that undergo reaction with either Brönsted or Lewis bases [59]. The Lewis acid character of pure TiO$_2$ is preserved upon adsorption of heavy-metal oxides such as Fe$_2$O$_3$ [60]. Wet-chemical titration of bulk anatase TiO$_2$ aqueous suspensions also indicated a continuous spectrum of the amphiphilic nature of surface OH-groups in TiO$_2$ spanning the range from strongly acidic to basic OH groups [13]. Numerous N-containing compounds such as NH$_3$, N$_2$H$_4$ and NH$_2$OH preferentially interact with Lewis acid sites in view of the confirmed absence of Brönsted acidity in pure anatase TiO$_2$ [59]. However, when titania contains contaminants such as SiO$_2$ significant Brönsted acidity may result. Taking on a slightly different viewpoint, Boehm and coworkers have stated that the density of acidic and basic OH-groups in titania (including TiO$_2$ P25) are roughly balanced [14]. Assuming titania to be pure it appears that N(CH$_3$)$_3$ directly interacts with TiO$_2$ as a Lewis acid akin to ammonia and hydroxylamine [61].

Hydroxylamine strongly interacts with Lewis acid sites of pure TiO$_2$ (anatase) despite the fact that it is a much weaker base than ammonia. Both the pK$_a$ in aqueous solution as well as the gas phase proton affinity PA are larger for NH$_3$ than for NH$_2$OH [28]: pK$_a$(NH$_3$) = 9.25, pK$_a$ (NH$_2$OH) = 5.96; PA(NH$_3$) = 854, PA(NH$_2$OH) = 803 kJ Mol^{-1}. Trimethylamine, N(CH$_3$)$_3$, is an even stronger base than NH$_3$ both in the gas phase as well as in aqueous

solution: $PA(N(CH_3)_3) = 942$ kJ Mol^{-1}, $pK_a(N(CH_3)_3) = 9.81$. This indicates that NH_2OH specifically reacts as a base with Lewis acid sites of TiO_2 in agreement with the fact that pure TiO_2 is not a Brönsted acid [59].

A look at Table 2 reveals a significant uptake of both $N(CH_3)_3$ and even more so of NH_2OH at ambient temperature on all three TiO_2 samples. A very efficient reaction of NH_2OH occurs on several formal monolayers of the TiO_2 substrate, at least for two of the investigated substrates, namely TiO_2 P25 and TiO_2 50. This means that hydroxylamine may undergo reaction with deeper layers of titania in subsurface reactions that have been well documented on TiO_2 single crystal surfaces [58]. In addition, the most reactive sample towards NH_2OH, TiO_2 P25, has been shown to contain traces of SiO_2 [59] whose Brönsted activity may contribute somewhat to its high reactivity towards hydroxylamine. The present data also indicate that $N(CH_3)_3$ and NH_2OH uptake is the smallest for TiO_2 with a high anatase content (TiO_2 15 nm) compared to a TiO_2 with a lower anatase content such as TiO_2 50. However, the anatase content given by the manufacturer *a priori* addresses the bulk composition which nevertheless does not preclude a systematic variation of the interface with the composition of the bulk. Under the present reaction conditions both N-containing compounds adsorb on the TiO_2 substrate until saturation with no observable products evolved at ambient temperature. We emphasize that NH_2OH apparently specifically reacts with bulk TiO_2 in contrast to combustion aerosol where the probe gas primarily interacts with aldehydes and ketones that are presumably part of the adsorbed organic phase of the carbonaceous aerosol.

As shown in Table 2 both acidic probes substantially interact with all three TiO_2 samples despite the fact that its Lewis acid character is well established [59]. Apparently, titania has the ability to bind acidic probe gases on basic sites akin to combustion aerosol particles owing to the presence of basic carbon oxides. Compared to the carbonaceous substrates the N_i^M(aerosol) values for CF_3COOH and HCl are large and of the same order of magnitude except for TiO_2 50 that has a ten times higher N_i^{HCl}(aerosol) value. In view of the fact that the generic TiO_2 surface is a Lewis rather than a Brönsted acid [59], we explain the fairly uniform reactivity towards CF_3COOH and HCl with the presence of surface hydroxyl groups that act as basic sites in agreement with results obtained by Flaig-Baumann [13]. The apparent exception, namely the titration of TiO_2 50 by a large amount of HCl, may be attributed to the formation of an oxychloride whose presence will have to be investigated in future experiments. Titration experiments in aqueous suspension of TiO_2 P25 reveal a strong adsorption of acetic acid, but

none with strong mineral acids such as HCl and HClO$_4$ [13]. A look at Table 2 shows that this trend is not borne out in the gas phase where there is even a slight preference for HCl adsorption compared to CF$_3$COOH. This is an example where the solution surface titration is different from the gas phase. This change in differential reactivity of CF$_3$COOH vs. HCl, the absence of any interaction of TiO$_2$ with gas phase NO$_2$ (see below) and the lack of CO$_2$ reaction on TiO$_2$ [62] are three examples for a change in reactivity of probe gases between the gas- and the condensed phase. In contrast, no differences in gas-condensed phase reactivities have so far been found for carbonaceous substrates.

TiO$_2$ does not interact with NO$_2$ in the gas phase despite its well-documented reactivity on single crystals [58], but reacts with gas phase O$_3$, most probably resulting in non-catalytic decomposition of ozone and generating O$_2$ [63-65]. Ozone reacts as a Lewis base and forms an adduct with titania which has Lewis acid character. In contrast, TiO$_2$ P25 reacts with NO$_2$ in solution to surface nitrate whose IR absorption has been identified [13]. Owing to the absence of significant amounts of adsorbed H$_2$O this reaction is thought to be a surface variant of the well-known disproportionation reaction leading to nitrate and nitrite according to 2NO$_2$ + H$_2$O → HNO$_3$ + HONO. The absence of a reaction in the gas phase as opposed to aqueous suspension may be attributed to the slow kinetics of disproportionation in the gas phase or at the interface. The O$_3$ uptake on TiO$_2$ is non-catalytic because it saturates after uptake of between 1.2 to 18 formal monolayers (Table 2). In addition, O$_2$ generation ceases after saturation of the O$_3$ uptake on TiO$_2$. It is conceivable that O$_3$ "fills" oxygen vacancies of the nanoparticle surface as well as subsurface vacancies in view of ist strong oxidizing power. No systematic trend between the anatase and rutile phase could be detected when considering the relative reactivities of all probe gases expressed by their N$_i^M$(aerosol) values. This is perhaps not too surprising as the specific structure is a property of the bulk of the particle whereas the present titration scheme specifically addresses the surface composition and structure.

Summary of Uptake Values

The surface reactivities of the different substrates based on the comparison of the N$_i^M$(aerosol) values for all six probe gases may be summarized as follows:

- Printex 60 has a significantly lower functional group density throughout, compared to other investigated carbonaceous substrates.
- FS 101 is a highly "reduced" combustion aerosol based on its reactivity with O$_3$.

- Diesel TPG aerosol particles are highly reactive except towards CF_3COOH which suggests that these nanoparticles do not have significant amounts of basic oxides. The surface density (N_i^M(aerosol)) of all other carbonaceous particles are comprised between the extremes of Printex 60 and Diesel TPG, representing the average minimum and maximum values of N_i^M, respectively.

- All three amorphous carbons together with lean hexane flame soot contain basic oxides as gauged by the larger N_i^M values for CF_3COOH than for HCl in contrast to other carbonaceous particles

- Due to the large number of surface functional groups which can be oxidized by O_3 and NO_2, laboratory soot from a hexane flame presents a "reduced" surface, akin to amorphous carbon FS 101.

- TiO_2 displays a large reactivity towards NH_2OH, CF_3COOH and HCl which is in agreement with the continuous distribution of acidic and basic OH groups on the surface of TiO_2. These go from Lewis acidic to Lewis basic character.

- On TiO_2 ozone decomposition is non-catalytic owing to rapid saturation of O_3 uptake and generates O_2 as a reaction product.

- Akin to Printex 60 TiO_2 15 has the lowest density of functional groups across all probe gases among the three studied TiO_2 samples despite the smallest size of its primary particles and the highest anatase content.

Uptake Kinetics.

Table 3 displays the initial uptake coefficients γ_0 that have been obtained from the MS data such as displayed in Figures 1 to 4 according to equations (1) and (2). As indicated above the γ_0 values have been obtained by using the geometric surface area (A_s) resulting in larger values of γ_0 compared to the same data normalized to the BET surface area because of the small geometric relative to the large BET surface area. A comparison between Tables 2 and 3 reveals that the uptake probability is roughly correlated with N_i^M(aerosol). The carbonaceous particles FW 2, SRM 2975 and Diesel TPG, taken as a group, have both high values of $N_i^{N(CH3)3}$ and N_i^{NH2OH} as well as large corresponding values γ_0. This relationship is expected because a high density of functional groups will lead to rapid uptake of the probe gas according to Equation (2). The uptake kinetics scales with the surface A_s of the substrate, everything else being equal. In addition, the γ_0 values of $N(CH_3)_3$ and NH_2OH for all carbonaceous particles are correlated which is also expected owing to the general acid

catalyzed nature of the oxime formation reaction, Equation (6): the higher the acidic group density (measured by $N_i^{N(CH3)3}$), the higher is the corresponding γ_0 and the faster is the oxime formation owing to the large catalyst concentration on the surface at a high value of $N_i^{N(CH3)3}$. A look at Table 2 and 3 provides further examples of such correlated behaviour between N_i^M and γ_0, such as $N_i^{CF3COOH}$ for FS 101, Printex 60 and FW2 or N_i^{HCl} for Diesel TPG. However, there are also exceptions, especially for O_3 as a probe gas. N_i^{O3} for Printex 60 γ_0 is unexpectedly large, whereas the reverse is true for N_i^{O3} for both hexane flame soots where γ_0 seems too small for the measured value of N_i^{O3}. When one considers the results for all three TiO_2 samples displayed in Table 3 one comes to the conclusion that there is also a rough correspondence of γ_0 with the bulk anatase content of TiO_2 in the order TiO_2 15 > TiO_2 P25 > TiO_2 50. In addition, the γ_0 values for HCl are in general larger compared to CF_3COOH uptake. The geometric area is the correct metric to use when dealing with the initial uptake probability γ_0 because the probe gas does not have the opportunity to explore the combined internal and external surface area in the short available reaction time, usually on the order of a few seconds or less. On the other hand, we are faced with considerable uncertainties of sample presentation when the masses of the substrates are as small as in the present work. We believe that the uptake probability γ_0 is an additional useful parameter to gauge the reactivity of aerosol surfaces towards probe gases.

Conclusions

The Knudsen cell is a suitable experimental tool for the characterization of the density of chemical surface functions of nanoparticles. The advantage of this technique compared to spectroscopic methods is that the obtained result is based on the particle surface **reactivity** towards different probe gases. Quantitative surface densities of functional groups are obtained in combination with a metric for the external surface of the nanoparticles. Such reactivity information is thought to be of prime importance to understand the potential toxicologic effects of nanoparticles. The following general observations may be made:

- The aerosol interface of the studied combustion and TiO_2 nanoparticles is **multifunctional,** combining acidic, basic, oxidizable [= reduced] and carbonyl functions on the same particle surface. The relative distribution of these surface groups may be a useful indicator for the state of oxidation in the case of a carbonaceous particle, and/or reactivity of a particle surface.

- The density of functional groups on the **carbonaceous** (combustion) **aerosol** surface is **variable** depending on the combustion conditions in contrast to the three investigated TiO_2 nanoparticle materials, whose surface shows a more uniform density of surface functional groups.

- A rough correlation exists between the uptake kinetics, expressed as the reaction probability per gas-surface collision, and the density of surface functional groups as expected from theory. However, there are also exceptions which indicate that there may be structural parameters also influencing the uptake kinetics.

Bibliographic References

1   *Intergovernmental Panel on Climate Change (IPCC)*, 2007, Geneva, Switzerland. (Available at http://www.ipcc.ch/ipccreports)

2   N. Künzli; R. Kaiser; S. Medina et al., *Lancet*, 2000, **356**, 795.

3   V. Ramanathan, P.J. Crutzen, J.T. Kiehl ,and D. Rosenfeld, *Science* 2001, **294**, 2119.

4   A. Nemmar; P.H. Hoet; B. Vanquickenborne; D. Dinsdale; M. Thomeer; M.F. Hoylaerts et al., *Circulation*, 2002, **105**, 411.

5   M. Geiser, B. Rothen-Rutishauser, N. Kapp, S. Schürch, W. Kreyling, H. Schulz, M. Semmler, V. Im Hof, J. Heyder and P. Gehr, *Environ. Health Persp.* 2005, **113**, 1555.

6   A.M. Schrand, H. Huang, C. Carlson, J.J. Schlager, E. Osawa, S.M. Hussain and L. Dai, *J. Phys. Chem. B* 2007, **111**, 2.

7   K. Donaldson, V. Stone, A. Clouter, L. Renwick and W. MacNee, *Occup. Environ. Med.* 2005, **58**, 211.

8   G. Oberdörster, E. Oberdörster and J. Oberdörster, *Env. Health Persp.* 2005, **113**, 823.

9   A. Baeza and F. Marano, *MS-Medecine Sciences* 2007, **23**, 497.

10   A. Baulig, M. Sourdeval, M. Meyer, F. Marano and A. Baeza-Squiban, *Toxicology in Vitro*, 2003, **17**, 567.

11   J.N. Smith and G.J. Rathbone, *Int. J. Mass Spectry*. 2008, **274**, 8.

12   A. Reff, B.J. Turpin, R.J. Porcja, R. Giovennetti, W.Q. Cui, C.P. Weisel, J. Zhang, J. Kwon, S. Alimokhtari, M. Morandi, T. Stock, S. Maberti, S. Colomé, A. Winer, D. Shendell, J. Jones and C. Farrar, *Indoor Air* 2005, **15**, 53.

13   R. Flaig-Baumann, M. Herrmann and H.P. Boehm, *Zeitschr, Anorg. Allg. Chem.* 1970, **372**, 296.

14   H.P. Boehm, *Carbon* 1994, **32**, 759.

15   H.P. Boehm, *Carbon*, 2002, **40**, 145.

16   A. Setyan, J.-J. Sauvain, M. Riediker, M. Guillemin and M.J. Rossi, *J. Aerosol. Sci.*. 2009, doi: 10.1016/j.jaerosci.2009.01.008.

17   D. M. Golden, G. N. Spokes and S.W. Benson, *Angew. Chem. IE* 1973, **12**, 534.

18   D. Stadler and M.J. Rossi, *Phys. Chem. Chem. Phys.* 2000, **2**, 5420.

19   F. Caloz, F.F. Fenter, K.D. Tabor and M.J. Rossi, *Rev. Sci. Instrum.* 1997, **68**, 3172.

20   Alcala-Jornod, C.; Rossi, M.J. *J. Phys. Chem. A* 2004, **108**, 10667.

21   A. Gerecke, A. Thielmann, L. Gutzwiller and M.J. Rossi, *Geophys. Res. Lett*. 1998, 25, 2453

22   *Handbook of Preparative Inorganic Chemistry*, 2nd edition, Vol. I, Brauer, G., ed., Academic Press, New York, p. 500, 1963.

23   S. Stephens, M.J. Rossi and D.M. Golden, *Int. J. Chem. Kinetics* 1986**, 18***,* 1133.

24   Handbook of Chemistry and Physics, 70th edition, R.C. Weast and D.R. Lide, eds., CRC Press, Inc., Boca Raton FL (1989-1990).

25   B. Demirdjian and M.J. Rossi, *Atmos. Chem. Phys. Discuss.* 2005, **5**, 607.

26   M.Z. Jacobson, H.C. Hansson, K.J. Noone and R.J. Charlson, *Rev. Geophys.* 2000, **38**, 267.

27   V.A. Lanz, M.R. Alfarra, U. Baltensperger, B. Buchmann, C. Hueglin, S. Szidat, M.N. Wehrli, L. Wacker, S. Weimer, A. Caserio, H. Puxbaum, A.S.H. Prévôt, *Environ. Sci. Technol.* 2008, **42**, 214.

28   *Modern Inorganic Chemistry*, W. L. Jolly, 2nd edition, McGraw Hill, New York 1991.

29   U. Hofmann and G. Ohlerich, *Angew. Chem.* 1950, **62**, 16.

30   H.P. Boehm and E. Diehl, *Zeitschr. Elektrochem.* 1962, **66**, 642.

31   H.P Boehm, E. Diehl, W. Heck and R. Sappok, *Angew. Chem.* 1964, **76**, 742.

32   H.P. Boehm, *Angew. Chem.* 1966, **78**, 617.

33   B.R. Larsen, D. Di Bella, M. Glasius, R. Winterhalter, N.R. Jensen and J. Hjorth, *J. Atmos. Chem.* 2004, **38**, 231.

34   X. Liu, M. Mason, K. Krebs and L. Sparks, *Env. Sci. Technol.* 2004, **38**, 2802.

35   Y. Ma, A.T. Russell and G. Marston, *Phys. Chem. Chem. Phys.* 2008, **10**, 4294.

36   A, Römpp, R. Winterhalter and G.K. Moortgat, *Atmos. Environ.* 2006, **40**, 6846.

37   J.-J. Sauvain, S. Deslarzes and M. Riediker, *Nanotoxicology* 2008, **2**, 121.

38   *Basic Principles of Organic Chemistry*, J.D. Roberts and M. C. Caserio, W. A. Benjamin, Inc., New York, 1965.

39   H.P. Boehm and M. Voll, *Carbon* 1970, **8**, 227.

40   M. Voll and H.P. Boehm, *Carbon*, 1970, **8**, 741.

41   M. Voll and H.P. Boehm, *Carbon*, 1971, **9**, 473.

42   M. Voll and H.P. Boehm, *Carbon*, 1971, **9**, 481.

43   *Chemistry of the Upper and Lower Atmosphere*, B.J. Finlayson-Pitts and J.N. Pitts, Jr., Academic Press, 2000.

44   F. Reisen and J. Arey, *Environ. Sci. Technol.* 2002, **36**, 4302.

45   R. Atkinson and S.M. Aschmann, *Int. J. Chem. Kin.* 1988, **20**, 513.

46   R. Atkinson, J. Arey and S.M. Aschmann, *Int. J. Chem. Kin.* 1992, **24**, 467.

47   E.C. Kwok, R. Atkinson and J. Arey, *Int. J. Chem. Kin.* 1997, **29**, 299.

48   E. Perraudin, H. Budzinski and E. Villenave, *J. Atm. Chem.* 2007, **56**, 57.

49   E. Perraudin, H. Budzinski and E. Villenave, *Atmos. Environ.* 2007, **41**, 6005.

50   T.F. Kahan, N.-O. A. Kwamena and D.J. Donaldson, *Atmos. Environ.* 2006, **40**, 3448.

51   N.-O. A. Kwamena, M.G. Staikova, D.J. Donaldson, I.J. George and J.P.D. Abbatt, *J. Phys. Chem. A* 2007, **111**, 11050.

52   W. Estève, H. Budzinski and E. Villenave, *Atmos. Environ.* 2006, **40**, 201.

53   E. Perraudin, H. Budzinski and E. Villenave, *Atmos. Environ.* 2005, **39**, 6557.

54   J.-O. Müller, D.S. Su, U. Wild and R. Schlögl, *Phys. Chem. Chem. Phys.* 2007, **9**, 4018.

55   H. Muckenhuber and H. Grothe, *Carbon* 2006, **44**, 546-559.

56   H. Muckenhuber and H. Grothe, *Carbon* 2007, **45**, 321-329.

57   G. Barco, A. Maranzana, G.Ghigo, M. Causà and G. Tonacchini, *J. Chem. Phys.* 2006, **125**, 194706.1-12.

58   U. Diebold, *Surf. Sci. Rep.* 2003, **48**, 53-229.

59   G. Busca, H. Saussey, O. Saur, J.C. Lavalley and V. Lorenzelli, *Appl. Catal.* 1985, **14**, 245.

60   M.A. Larrubia, G. Ramis and G. Busca, *Appl. Catal. B: Environm.* 2001, **30**, 101.

61   G. Ramis, M.A. Larrubia and G. Busca, *Topics in Catalysis*, 2000, **11/12**, 161.

62   The lack of uptake of gas phase CO_2 with TiO_2 15 and 50 is in stark contrast to the significant interaction of HCO_3^- with aqueous suspensions of TiO_2 P25 [13]. Although not systematically used as a surface probe in the present investigation, we stress that the behaviour of CO_2 towards the TiO_2 samples is different in the gas and condensed phase.

63   S.T. Oyama, *Catal. Rev.-Sci Eng.* 2000, **42**, 279.

64   K.M. Bulanin, J.C. Lavalley and A.A. Tsyganenko, *J. Phys. Chem.* 1995, **99**, 10294.

65   R. Radakrishnan and S.T. Oyama, *J. Catal.* 2001, **199**, 282.

Table 1 Knudsen flow reactor parameters for the 1mm nominal diameter aperture.

Parameter[a]	Value
Volume of the reactor	V = 1830 [cm^3]
Estimated surface area of the reactor	S = 1300 [cm^2]
Geometric surface area of the samples	A$_s$ = 12.6 [cm^2] for both hexane soot samples A$_s$ = 3.14 [cm^2] for FS 101, Printex 60, FW 2, SRM 2975, Diesel TPG and TiO$_2$ samples
Escape orifice diameter	Ø = 1 [mm]
Chopper frequency	225 [Hz]
Concentration of gas-phase probes in the reactor	10^{13} [molecule/cm^3]
Molecular flow rate of gas-phase probes	5 · 10^{14} [molecule/sec]
Escape rate constant	k$_{esc}$ = 0.010 · $\sqrt{T/M}$ [s^{-1}]

[a]T = temperature [K], M = molecular mass [g/mol].

Table 3. Initial uptake coefficient γ_0 of heterogeneous chemical reactions between gas phase probe molecules and supported aerosol nanoparticles obtained using the Knudsen flow reactor based on the geometric surface area of the sample support. Values in brackets correspond to the standard deviation of duplicates.

	N(CH$_3$)$_3$	NH$_2$OH	CF$_3$COOH	HCl	O$_3$	NO$_2$
FS 101	7.8 (±0.4) · 10^{-4}	6.1 (±1.0) · 10^{-4}	7.9 (±0.6) · 10^{-3}	no reaction	1.1 (±0.1) · 10^{-2}	3.8 (±0.3) · 10^{-4}
Printex 60	9.9 (±0.6) · 10^{-4}	9.9 (±1.7) · 10^{-4}	2.2 (±0.2) · 10^{-2}	2.1 (±0.1) · 10^{-3}	1.0 (±0.1) · 10^{-1}	1.8 (±0.2) · 10^{-3}
FW 2	4.3 (±0.2) · 10^{-2}	4.4 (±0.7) · 10^{-2}	1.6 (±0.1) · 10^{-2}	no reaction	1.1 (±0.1) · 10^{-1}	5.8 (±0.5) · 10^{-3}
SRM 2975	2.4 (±0.1) · 10^{-2}	1.5 (±0.3) · 10^{-2}	no reaction	2.9 (±0.1) · 10^{-3}	5.8 (±0.5) · 10^{-4}	6.3 (±0.5) · 10^{-4}
Diesel TPG	1.3 (±0.1) · 10^{-2}	2.1 (±0.4) · 10^{-2}	no reaction	1.3 (±0.1) · 10^{-2}	1.0 (±0.1) · 10^{-2}	1.4 (±0.1) · 10^{-3}
Hexane rich flame	8.4 (±0.5) · 10^{-5}	4.2 (±0.7) · 10^{-4}	3.6 (±0.3) · 10^{-4}	2.0 (±0.1) · 10^{-4}	1.6 (±0.1) · 10^{-3}	2.8 (±0.2) · 10^{-3}
Hexane lean flame	8.7 (±0.5) · 10^{-5}	1.5 (±0.3) · 10^{-3}	2.9 (±0.2) · 10^{-3}	1.7 (±0.1) · 10^{-4}	2.4 (±0.2) · 10^{-2}	2.5 (±0.2) · 10^{-3}
TiO$_2$ 15	2.5 (±0.1) · 10^{-1}	8.4 (±1.4) · 10^{-2}	5.5 (±0.4) · 10^{-2}	1.4 (±0.1) · 10^{-1}	1.0 (±0.1) · 10^{-3}	no reaction
TiO$_2$ 50	6.5 (±0.4) · 10^{-3}	1.5 (±0.3) · 10^{-2}	1.0 (±0.1) · 10^{-2}	1.9 (±0.1) · 10^{-2}	6.4 (±0.5) · 10^{-4}	no reaction
TiO$_2$ P25	4.5 (±0.3) · 10^{-2}	5.9 (±1.0) · 10^{-2}	3.5 (±0.3) · 10^{-2}	1.5 (±0.1) · 10^{-1}	1.5 (±0.1) · 10^{-3}	no reaction

Table 2 Uptake N_i(aerosol) of six probe gases in molecular units. Values displayed in first, second and third row of each box correspond to uptake per mg, per cm^2 of substrate and to a formal molecular monolayer in % (see text), respectively. Typical uncertainty derived from duplicates is ± 15% for all three entries per box.

	Surface BET [m²/g]	N(CH₃)₃	NH₂OH	CF₃COOH	HCl	O₃	NO₂
FS 101	20[a]	$5.8 \cdot 10^{14}$ $2.9 \cdot 10^{12}$ 0.81	$1.2 \cdot 10^{16}$ $6.0 \cdot 10^{13}$ 7.6	$1.8 \cdot 10^{15}$ $9.2 \cdot 10^{12}$ 2.3	No reaction	$7.3 \cdot 10^{17}$ $3.7 \cdot 10^{15}$ 498.0	$2.0 \cdot 10^{15}$ $9.8 \cdot 10^{12}$ 1.4
Printex 60	115[a]	$1.5 \cdot 10^{15}$ $1.3 \cdot 10^{12}$ 0.36	$2.1 \cdot 10^{16}$ $1.8 \cdot 10^{13}$ 2.3	$4.0 \cdot 10^{15}$ $3.5 \cdot 10^{12}$ 0.9	$8.2 \cdot 10^{14}$ $7.1 \cdot 10^{11}$ 0.08	$6.4 \cdot 10^{16}$ $5.6 \cdot 10^{13}$ 7.5	$7.4 \cdot 10^{15}$ $6.4 \cdot 10^{12}$ 0.90
FW 2	460[a]	$2.4 \cdot 10^{17}$ $5.2 \cdot 10^{13}$ 14.5	$4.4 \cdot 10^{17}$ $9.6 \cdot 10^{13}$ 12.2	$4.5 \cdot 10^{16}$ $9.9 \cdot 10^{12}$ 2.5	No reaction	$4.4 \cdot 10^{17}$ $9.6 \cdot 10^{13}$ 12.9	$4.1 \cdot 10^{16}$ $8.9 \cdot 10^{12}$ 1.3
SRM 2975	91	$4.9 \cdot 10^{16}$ $5.3 \cdot 10^{13}$ 14.7	$1.3 \cdot 10^{18}$ $1.5 \cdot 10^{15}$ 191.1	No reaction	$2.4 \cdot 10^{15}$ $2.6 \cdot 10^{12}$ 0.3	$8.3 \cdot 10^{15}$ $9.1 \cdot 10^{12}$ 1.2	$3.2 \cdot 10^{15}$ $3.5 \cdot 10^{12}$ 0.49
Diesel TPG	53.2[f]	$3.1 \cdot 10^{16}$ $5.8 \cdot 10^{13}$ 16.1	$1.4 \cdot 10^{18}$ $2.6 \cdot 10^{15}$ 331.2	No reaction	$4.6 \cdot 10^{16}$ $8.7 \cdot 10^{13}$ 10.1	$1.3 \cdot 10^{17}$ $2.5 \cdot 10^{14}$ 33.7	$1.3 \cdot 10^{16}$ $2.4 \cdot 10^{13}$ 3.38
Hexane soot from rich flame	48.9[f]	$1.8 \cdot 10^{15}$ $3.8 \; 10^{12}$ 1.1	$2.1 \cdot 10^{17}$ $4.4 \; 10^{14}$ 55.7	$1.8 \cdot 10^{15}$ $3.8 \; 10^{12}$ 0.9	$9.0 \cdot 10^{15}$ $1.9 \; 10^{13}$ 2.2	$9.5 \cdot 10^{17}$ $2.0 \; 10^{15}$ 266.4	$2.6 \cdot 10^{16}$ $5.4 \; 10^{13}$ 7.6
Hexane soot from lean flame	74.3[f]	$2.8 \cdot 10^{15}$ $3.8 \; 10^{12}$ 1.1	$3.3 \cdot 10^{17}$ $4.5 \; 10^{14}$ 56.8	$3.2 \cdot 10^{15}$ $4.3 \; 10^{12}$ 1.1	$3.1 \cdot 10^{15}$ $4.2 \; 10^{12}$ 0.5	$2.0 \cdot 10^{18}$ $2.7 \; 10^{15}$ 364.0	$1.9 \cdot 10^{16}$ $2.6 \; 10^{13}$ 3.6
[c]**TiO₂ 15**	210±10[b]	$1.4 \cdot 10^{17}$ $6.6 \cdot 10^{13}$ 18.3	$2.7 \cdot 10^{18}$ $1.1 \cdot 10^{15}$ 140.1	$1.1 \cdot 10^{17}$ $5.3 \cdot 10^{13}$ 13.1	$3.9 \cdot 10^{17}$ $1.9 \cdot 10^{14}$ 22.1	$1.9 \cdot 10^{16}$ $9.1 \cdot 10^{12}$ 1.2	No reaction
[d]**TiO₂ 50**	21.4[b]	$3.2 \cdot 10^{16}$ $1.5 \cdot 10^{14}$ 41.7	$1.5 \cdot 10^{18}$ $7.0 \cdot 10^{15}$ 892	$1.2 \cdot 10^{16}$ $5.7 \cdot 10^{13}$ 14.1	$3.9 \cdot 10^{17}$ $1.8 \cdot 10^{15}$ 209.3	$7.1 \cdot 10^{15}$ $3.3 \cdot 10^{13}$ 4.44	No reaction
[e]**TiO₂ P25**	50±15[a]	$6.4 \cdot 10^{16}$ $1.3 \cdot 10^{14}$ 36.1	$3.9 \cdot 10^{18}$ $7.7 \cdot 10^{15}$ 981	$1.1 \cdot 10^{16}$ $2.3 \cdot 10^{13}$ 5.7	$1.4 \cdot 10^{17}$ $2.8 \cdot 10^{14}$ 32.6	$6.4 \cdot 10^{16}$ $1.3 \cdot 10^{14}$ 17.5	No reaction

[a] Data given by manufacturer (Evonik AG)
[b] Data given by manufacturer (Sigma-Aldrich AG)
[c] TiO₂ 15 nm : 98% anatase, 2% rutile (bulk)

[d] TiO₂ 50 nm : 65% anatase, 35% rutile (bulk)
[e] TiO₂ P25: 80-90% anatase, balance rutile (bulk).
[f] Determined at EPFL (see under Experimental).

Figure Captions

Figure 1. Raw data of CF_3COOH uptake on 1.77 mg of amorphous carbon FW 2 at a flow rate of 2.8 x 10^{14} molecule s^{-1} monitored at m/e 45 in the 1 mm diameter aperture Knudsen flow reactor (k_{esc} = 0.0214 s^{-1}) leading to the initial uptake coefficient γ_0 = 3.9 x 10^{-3}.
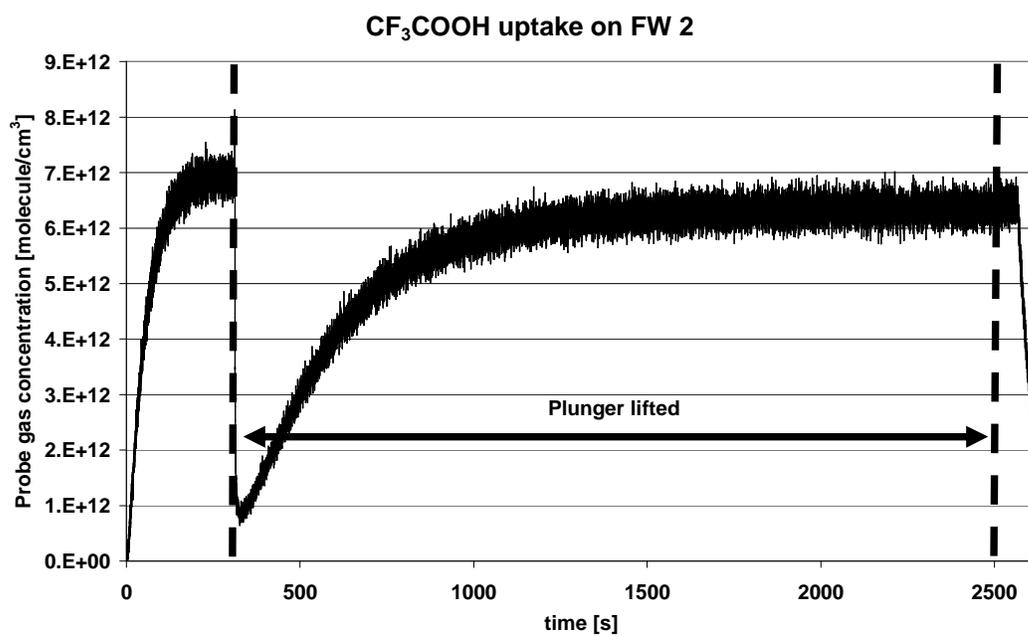
Figure 2. Raw data of HCl uptake on 1.93 mg of TiO_2 P25 powder at a flow rate of 9.4 x 10^{14} molecule s^{-1} monitored at m/e 36 in the 1 mm diameter aperture Knudsen flow reactor (k_{esc} = 0.0443 s^{-1}) leading to the initial uptake coefficient γ_0 = 3.7 x 10^{-3}.

Figure 3. Raw data of $N(CH_3)_3$ uptake on 10.0 mg amorphous carbon FS 101 at a flow rate of 6.4 x 10^{14} molecule s^{-1} monitored at m/e 58 in the 1 mm diameter aperture Knudsen flow reactor (k_{esc} = 0.0308 s^{-1}) leading to the initial uptake coefficient γ_0 = 2.0 x 10^{-4}.

Figure 4. Raw data of O_3 uptake on 1.14 mg of soot from a rich hexane flame at a flow rate of 6.7 x 10^{15} molecule s^{-1} monitored at m/e 48 in the 1 mm diameter aperture Knudsen flow reactor (k_{esc} = 0.0509 s^{-1}) leading to the initial uptake coefficient γ_0 = 1.6 x 10^{-3}.
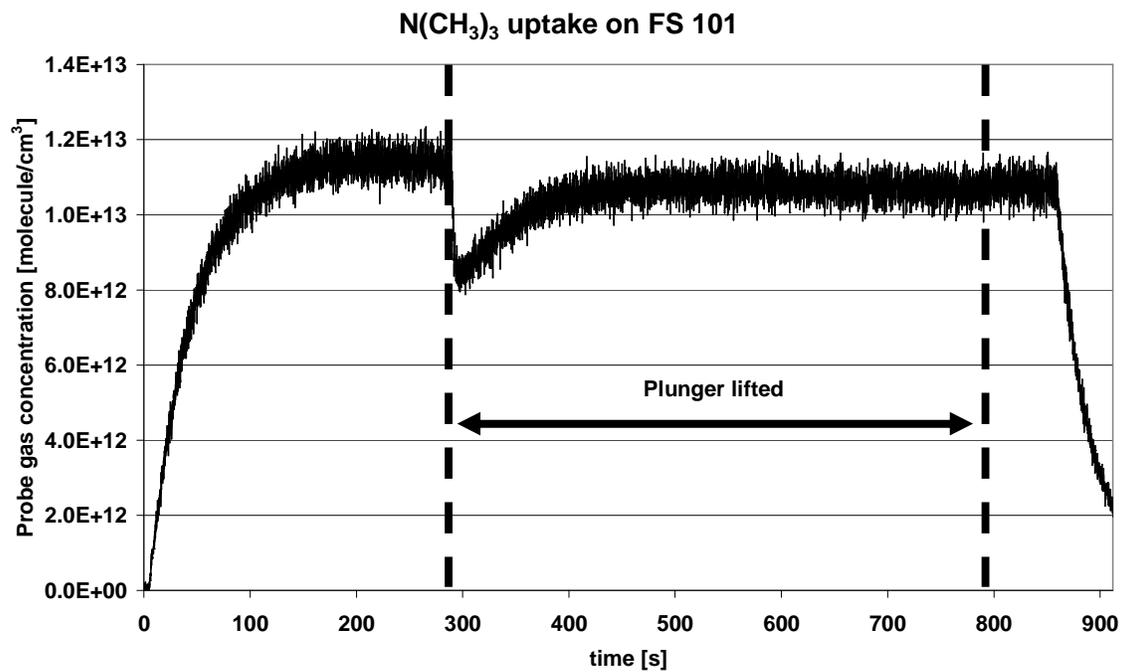
CF₃COOH uptake on FW 2

Fig. 1

HCl uptake on TiO₂ P25

Fig. 2

N(CH$_3$)$_3$ uptake on FS 101

Probe gas concentration [molecule/cm^3]

time [s]

Plunger lifted

Fig. 3

O$_3$ vs hexane soot rich flame
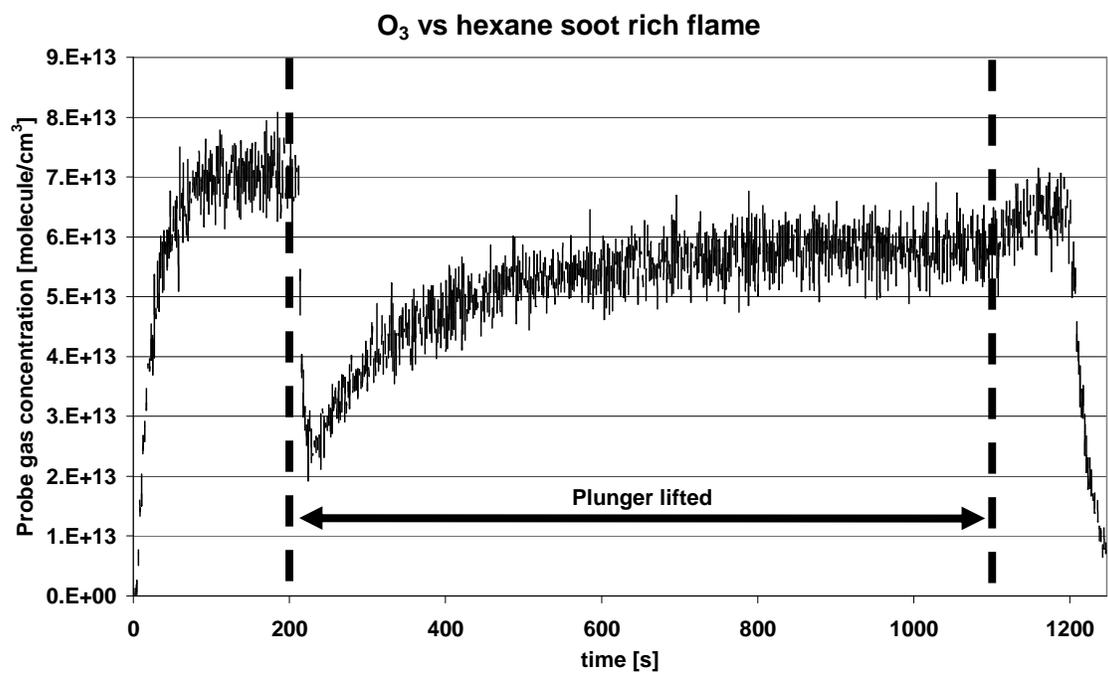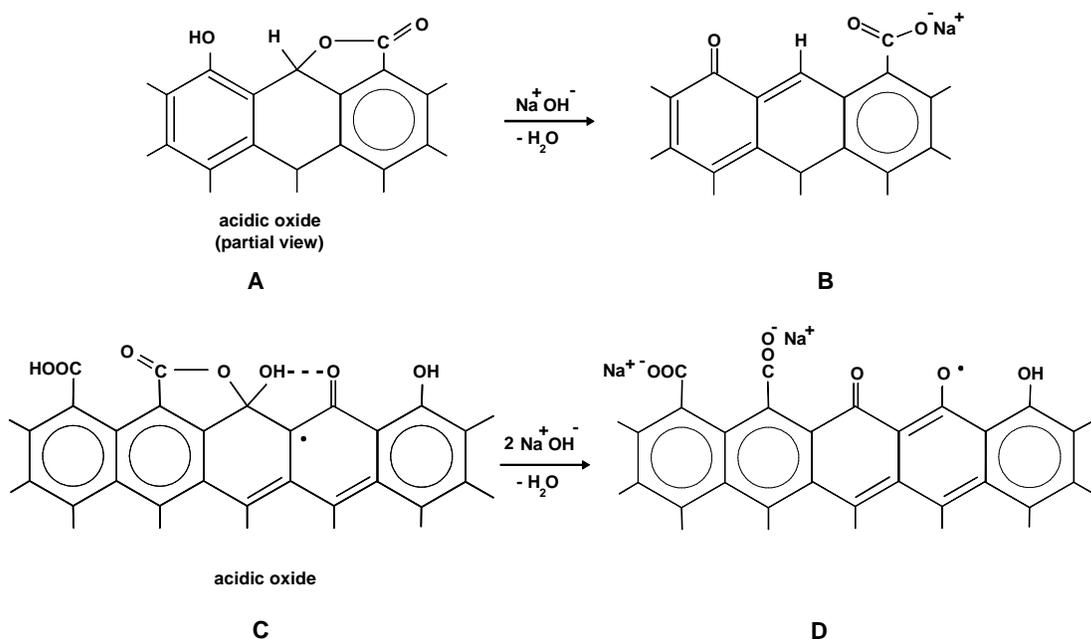
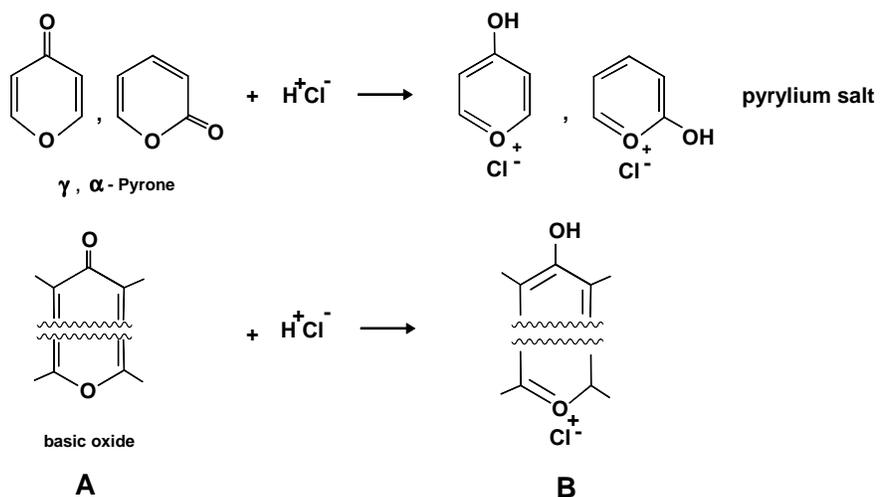Probe gas concentration [molecule/cm^3]

time [s]

Plunger lifted
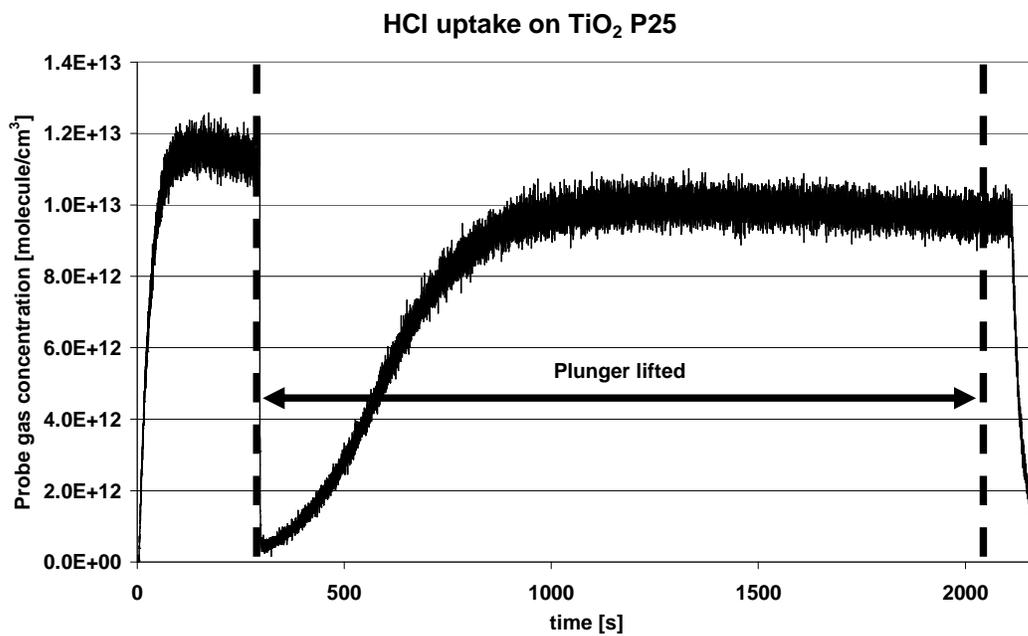
Fig. 4

Scheme I (Carbonaceous surface acidic oxide neutralization)

Scheme II (Carbonaceous surface basic oxide neutralization. The wavy line in the formula of Scheme II indicates that both O-functionalities are not required to be part of the same aromatic ring system but may be separated by one or several aromatic rings.)